

Robust zero modes in PbTe-Pb hybrid nanowires

Shan Zhang,^{1,*} Wenyu Song,^{1,*} Zonglin Li,^{1,*} Zehao Yu,^{1,*} Ruidong Li,¹ Yuhao Wang,¹ Zeyu Yan,¹ Jiaye Xu,¹ Zhaoyu Wang,¹ Yichun Gao,¹ Shuai Yang,¹ Lining Yang,¹ Xiao Feng,^{1,2,3,4} Tiantian Wang,^{2,4} Yunyi Zang,^{2,4} Lin Li,² Runan Shang,^{2,4} Qi-Kun Xue,^{1,2,3,4,5} Ke He,^{1,2,3,4,†} and Hao Zhang^{1,2,3,‡}

¹State Key Laboratory of Low Dimensional Quantum Physics,

Department of Physics, Tsinghua University, Beijing 100084, China

²Beijing Academy of Quantum Information Sciences, Beijing 100193, China

³Frontier Science Center for Quantum Information, Beijing 100084, China

⁴Hefei National Laboratory, Hefei 230088, China

⁵Southern University of Science and Technology, Shenzhen 518055, China

Majorana zero modes in tunneling conductance are expected to manifest as robust zero bias peaks (ZBPs). While ZBPs alone are not conclusive evidence of Majorana modes due to alternative explanations, robust ZBPs remain a crucial and necessary first-step indicator in the search for topological states. Here, we report the observation of robust ZBPs in PbTe-Pb hybrid nanowires. The peak height can reach $2e^2/h$, though it does not yet form a quantized plateau. Importantly, these ZBPs can remain non-split over sizable ranges in both magnetic field and gate voltage scans, highlighting their robustness. We discuss possible interpretations based on Majorana zero modes as well as Andreev bound states.

The search for Majorana zero modes in semiconductor-superconductor hybrid nanowires has driven a decade of intense research activities due to its potential applications in topological quantum computation [1–5]. While significant experimental progress has been made [6–15], deeper insights into these hybrid nanowires have highlighted disorder as the primary challenge [16–23]. This understanding has led to a shift in the community perspective. Currently, the consensus is that zero bias peaks (ZBPs) observed in local tunneling conductance measurements are a necessary but not sufficient signature of Majorana zero modes. One dominating alternative explanation is the presence of Andreev bound states (ABSs), which are common in the same material system [24]. These ABSs can be fine-tuned to zero energy, mimicking the Majorana signatures.

To conclusively establish the existence of Majoranas, a braiding experiment demonstrating non-Abelian statistics is required. Braiding also serves as a key ingredient in quantum gate operations for topological qubits. Such experiments demand network structures of nanowire devices [25–27]. Most ZBP experiments so far have utilized free-standing InAs and InSb nanowires grown via the vapor-liquid-solid (VLS) method. However, the scalability of VLS-grown nanowires is limited, hindering their further application toward complex networks. Selective-area-grown (SAG) nanowires can address this issue, as networks can be defined through electron-beam lithography and grown on demand [28–30]. However, disorder introduced by lattice mismatch at the nanowire/substrate interface severely degrades the quality of SAG nanowires. To date, robust ZBPs have not been reported in SAG devices.

Besides the semiconductor part, the choice of superconductor is another critical consideration. Most ZBP experiments have relied on aluminum, which has a small superconducting gap, a low g -factor, and weak spin-orbit interaction, yielding undesired metalization effects [31]. In recent years, numerous alternative superconductors such as Pb, Sn, In and Ta have been explored with high expectations [32–35]. However, robust ZBPs comparable in quality to those in Al-based hybrids have not yet been observed in these new material systems. The absence of robust ZBPs in SAG nanowires and alternative superconductor hybrids remains a major roadblock. Addressing this challenge is essential for the next stage of progress toward scalable topological quantum computing.

Here, we address this challenge by demonstrating robust zero-bias peaks in SAG PbTe-Pb hybrid nanowires. PbTe has recently emerged as a promising alternative to InAs and InSb due to its reduced disorder [36]. These nanowire hybrids have been systematically grown and characterized [37–52]. The observation of robust ZBPs in this study marks a crucial step toward realizing Majorana zero modes in this emerging hybrid system.

Figure 1(a) shows a scanning electron micrograph (SEM) of a PbTe-Pb nanowire (device A). Details of the growth and device fabrication can be found in our previous works [47, 52]. The lower panel provides a schematic illustration (not to scale). For clarity, the substrate CdTe/Pb_{0.99}Eu_{0.01}Te is not shown. The PbTe-Pb wire was capped in situ with a thin CdTe layer (cyan). During device fabrication, a thin dielectric layer of Al₂O₃ (green) was deposited via atomic layer deposition, followed by the evaporation of two top gates: a tunneling gate (TG) and a “superconducting region gate” (SG). The TG controls the transmission probability of the “barrier region”, which is the PbTe segment without Pb coverage. The SG modulates the carrier density in the proximitized PbTe region (with Pb coverage). Note that due to Pb screening effects, the SG top gate effectively acts as a side gate.

* equal contribution

† kehe@tsinghua.edu.cn

‡ hzquantum@mail.tsinghua.edu.cn

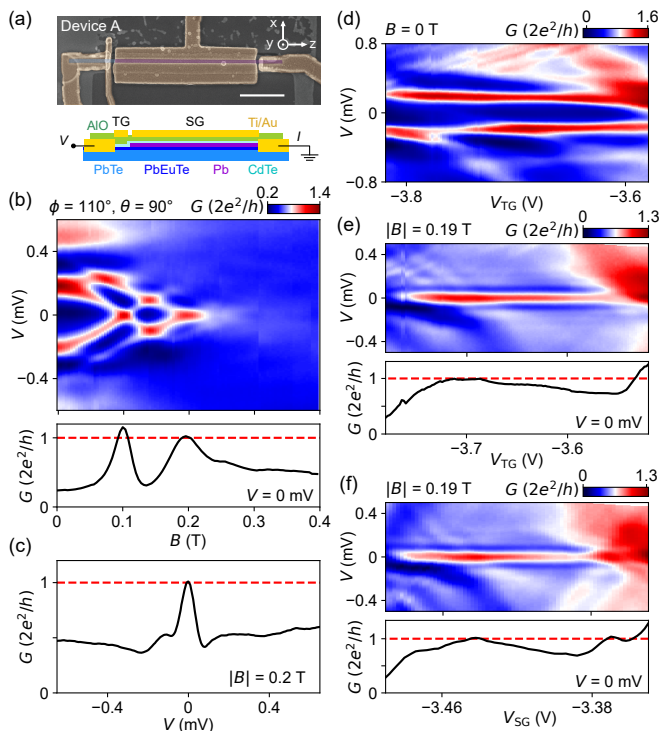


FIG. 1. Robust ZBPs in device A. (a) False-color SEM (upper) and device schematic (lower). Scale bar, 1 μm . (b) B scan of a ZBP. $V_{TG} = -3.714$ V, $V_{SG} = -3.4631$ V. $\phi = 110^\circ$, $\theta = 90^\circ$. Lower panel, zero-bias line cut. (c) A line cut from (b) at 0.2 T. (d) G vs V and V_{TG} at 0 T. $V_{SG} = -3.4631$ V. (e) TG scan of the ZBP at 0.19 T. $V_{SG} = -3.444$ V. Lower panel, zero-bias line cut. (f) SG scan of the ZBP at 0.19 T. $V_{TG} = -3.69$ V. Lower panel, zero-bias line cut. The orientations of B in (e-f) are the same with that in (b).

Standard two-terminal tunneling spectroscopy was performed in a dilution fridge at a base temperature below 50 mK. We measured the differential conductance, $G \equiv dI/dV$, as a function of magnetic field (B) and gate voltages (V_{TG} and V_{SG}). The contributions from fridge filters have been excluded from both G and the bias voltage V .

We then search ZBPs in the (B, V_{TG}, V_{SG}) parameter space. Figure 1(b) depicts an example found at a particular gate setting. The orientation of B is perpendicular to the nanowire and will be discussed in detail in Fig. 2. At zero field, we observe two prominent peaks at $V \sim \pm 0.2$ mV, located within the induced superconducting gap. The gate dependence of the gap is detailed in Fig. S1 of the Supplementary Material (SM). The induced gap, estimated to be around 0.5 meV, is significantly smaller than the bulk gap of Pb (~ 1 meV). This reduction in gap size is achieved by introducing a 4-nm-thick Pb_{0.97}Eu_{0.03}Te interlayer between PbTe and Pb (the dark blue layer in Fig. 1(a)). As B increases, the subgap peaks quickly split and cross zero energy at 0.1 T, where a ZBP appears. However, this ZBP is non-robust and quickly splits at higher B 's, indicating its trivial na-

ture [24]. More notably, a robust ZBP emerges for B between 0.18 T and 0.28 T, persisting without splitting until the gap closes. This evolution — a non-robust ZBP followed by a robust ZBP — resembles numerical simulations from Ref. [53], where the non-robust and robust ZBPs correspond to ABS and Majoranas, respectively. We note that robustness in local tunneling spectroscopy is a necessary but not sufficient indicator of Majoranas.

The peak height of the non-robust ZBP exceeds $2e^2/h$, whereas for the robust ZBP, it initially reaches $2e^2/h$ first before decreasing as B increases. The lower panel of Fig. 1(b) shows the zero-bias line cut, illustrating this evolution. Figure 1(c) highlights the ZBP at $2e^2/h$. However, this ZBP is not quantized, as its peak height does not form a plateau in the B scan. We note that quantization is not definitive evidence either, given alternative mechanisms such as quasi-Majoranas [54, 55]. For waterfall plots of Fig. 1(b), see Fig. S1. Figure S2 presents further B scans at different gate settings.

In Fig. 1(d), we scan V_{TG} near this parameter regime at $B = 0$ T. The two subgap peaks exhibit minimal modulation, whereas the conductance outside the gap varies with V_{TG} , likely due to Fabry-Pérot-like oscillations or the formation of unintentional quantum dots near the barrier. Figures 1(e-f) display the TG and SG scans at 0.19 T, where the ZBP remains robust (i.e. non-split) across a broad parameter range, unaffected by the modulations from dot states. The lower panels illustrate zero-bias line cuts, showing the evolution of peak height. Although the height can reach $2e^2/h$, it does not form a plateau. For gate scans of this ZBP over a larger parameter range, we refer to Fig. S1 in SM.

We next examine the robustness of this ZBP by rotating the B direction, as shown in Figs. 2(a-c). The coordinate axes are defined schematically in Fig. 2(d): the z axis is parallel to the wire, the y axis is out of plane, the x axis is perpendicular to the wire and in-plane, θ is the angle between B and the z axis, ϕ is the angle between the x axis and the B component in the xy plane. Figures 2(a-b) show the B rotation in the xy and yz planes while maintain a fixed magnitude of $|B|$ at 0.196 T. For rotation in the xz plane, see Fig. S3 in SM. The ZBP remains robust over an angle range of 50° in both the xy and yz planes. For rotation in the xy plane, the “central direction” of the ZBP slightly misaligned with the y axis, occurring at $\phi > 90^\circ$). We thus set $\phi = 110^\circ$ ($\theta = 90^\circ$) for the B direction in Fig. 1 — corresponding to an orientation 20° away from the y axis in the xy plane. Figure 2(c) presents a θ scan while holding ϕ fixed at 110° , again revealing a robust ZBP. For additional rotation data and corresponding waterfall plots, see Fig. S3 in SM.

As B rotates beyond the robust regions, the ZBP splits and subsequently merges back, forming a non-robust ZBP. This non-robust ZBP in Fig. 2(a) locates between the x and y axes at $\phi \sim 40^\circ$. When B is further aligned with the x axis, the non-robust ZBP splits into two subgap peaks. This angular dependence resembles the behavior of $|B|$ scan in Fig. 1(b). The underlying mech-

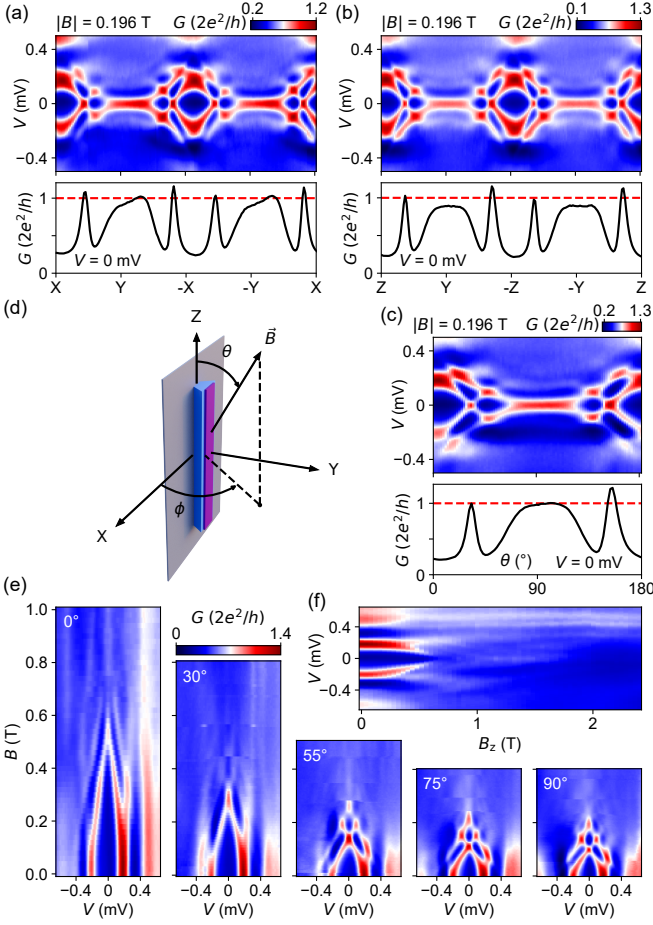


FIG. 2. Angle dependence of the ZBP. (a-b) B rotations in the xy (rotating ϕ) and yz (rotating θ) planes. $|B| = 0.196$ T. Lower panels, zero-bias line cuts. (c) B rotation by fixing $\phi = 110^\circ$ and varying θ . $V_{TG} = -3.714$ V and $V_{SG} = -3.4631$ V for (a-c). (d) Schematic illustration of the coordinate axes, ϕ , and θ . (e) B scans of the ZBP. $\theta = 90^\circ$. ϕ is fixed from left to right at 0° , 30° , 55° , 75° , and 90° , respectively. $V_{TG} = -3.73$ V and $V_{SG} = -3.48$ V for the middle 3 panels. (f) B_z scan. $V_{TG} = -3.714$ V and $V_{SG} = -3.456$ V for (f) and the left panel of (e). For the right panel of (e), $V_{SG} = -3.444$ V.

anism is the g -factor anisotropy in PbTe-Pb nanowires [52]. Specifically, in Fig. 2(a), the effective g -factor is small when B is along the x axis ($\phi = 0^\circ$) and significantly larger when B is along the y axis ($\phi = 90^\circ$). As a result, the effective Zeeman splitting increases as B rotates from $\phi = 0^\circ$ to 90° . For the case of Fig. 1(b), the Zeeman splitting is tuned by the magnitude of B rather than its direction (g -factor anisotropy).

To reveal this anisotropy, we performed B scans along different directions, as shown in Fig. 2(e). θ is fixed at 90° , while ϕ varies successively for each panel from 0° (the x axis) to 30° , 55° , 75° , and 90° (the y axis). The onset field of the ZBP decreases with increasing ϕ , indicating a decrease in the g -factor. Based on the slopes of the peak dispersion in B , we estimate the g -factors for these five directions to be 15, 27, 55, 75, and 81, respec-

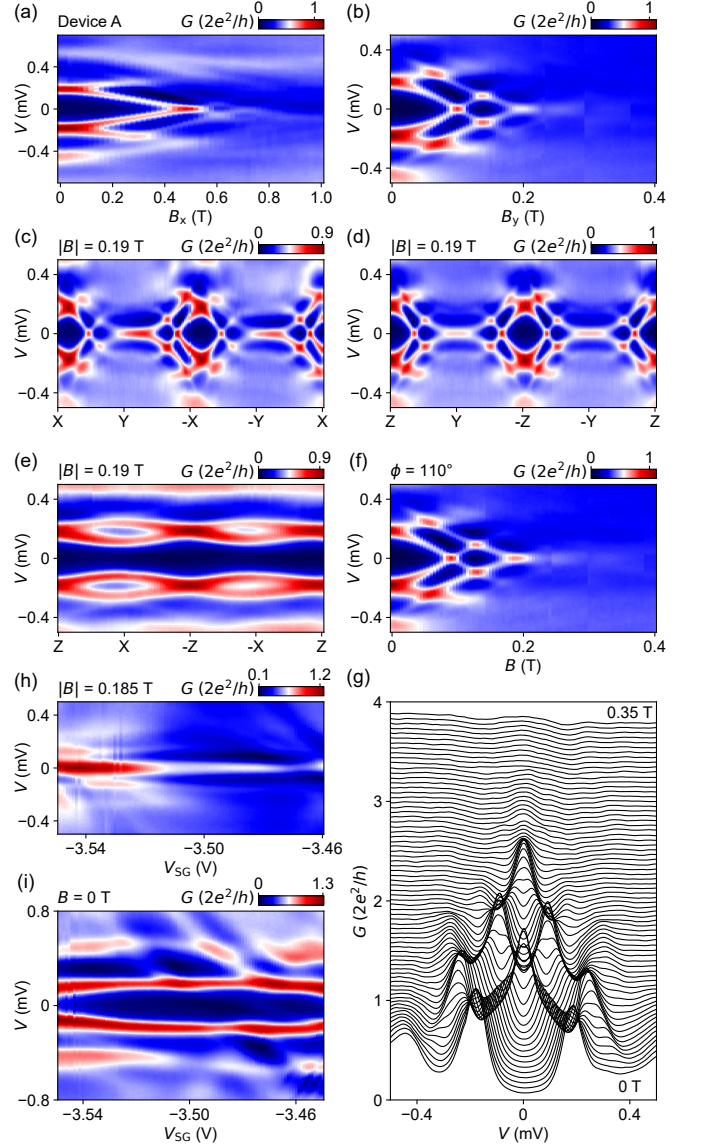


FIG. 3. Robust ZBP in a different parameter space of device A. (a-b) B_x and B_y scans of the ZBP. (c-e) B rotations in the xy , yz , and xz planes. $|B| = 0.19$ T. (f) B scan of the ZBP by fixing θ at 90° and ϕ at 110° . For (a-f): $V_{TG} = -3.57$ V, $V_{SG} = -3.496$ V. (g) Waterfall plot of (f) with a vertical offset ($0.05 \times 2e^2/h$) for clarity. (h-i) SG scans at 0.185 T ($\theta = 90^\circ$, $\phi = 110^\circ$) and 0 T, respectively. $V_{TG} = -3.57$ V.

tively. For the $\phi = 0^\circ$ case (the x axis), the ZBP persists over a broad field range, from 0.52 T to 1 T, without splitting. This suggests that the non-robust ZBP in Fig. 1(b) transitions smoothly into the robust one, without a distinct splitting event. Similar behavior has been revealed in numerical simulations [56], where an ABS can continuously evolve into a Majorana state without anything noticeable at the transition point. Figure 2(f) presents the B_z scan, where the g -factor is even smaller (~ 11). As a result, no ZBP is observed before the gap closure. However, a faint ZBP appears after the gap has closed,

which is likely disorder-induced [16].

Figures 1-2, along with the related supplemental figures, constitute a complete dataset of a ZBP. In Figure 3, we present a second dataset, also measured in device A but within a different region of the parameter space. A significant charge jump occurred between the measurements of these two datasets, making direct comparisons of gate settings less meaningful. Figures 3(a-b) display the B_x and B_y scans of the ZBP. The estimated g -factors are 14 and 79, respectively. Consequently, the first crossing point (the non-robust ZBP) occurs at a higher B in the B_x scan compared to B_y . Unlike the B_x scan in Fig. 2(e) ($\phi = 0^\circ$), the non-robust ZBP in Fig. 3(a) (near 0.5 T) quickly splits and does not evolve into a robust one. The B_y scan in Fig. 3(b) reveal a robust ZBP. The height of this robust ZBP — $\sim 0.65 \times 2e^2/h$ — is significantly lower than the quantized value. For completeness, Fig. S4 shows the B_z scan, where no ZBP is observed.

We then fixed the B amplitude at 0.19 T and rotated the B direction in the planes, as shown in Figs. 3(c-e). Similar to Figs. 2(a-b), the ZBP remains robust over a considerable angular range in xy and yz planes. No ZBP is observed in the xz plane due to a relatively small g -factor. Based on these rotations, we identify $\phi = 110^\circ$ and $\theta = 90^\circ$ as the “sweet spot” orientation. Figure 3(d) presents the B scan along this direction, with its waterfall plot shown in Fig. 3(g). The ZBP remains stable from 0.175 T to 0.29 T. Figure 3(h) further illustrates the robustness of this ZBP in the SG scan at $B = 0.185$ T (for the TG scan, see Fig. S4). Notably, at zero field, the same SG scan reveals no ZBP, as shown in Fig. 3(i).

For reproducibility purpose, we show robust ZBPs in a second PbTe-Pb device in Figure 4. Figure 4(b) depicts its false-colored SEM. At zero field, the tunneling spectroscopy in Fig. 4(a) reveals a superconducting gap (size near 0.5 meV) with many Andreev states due to formation of unintentional quantum dots. Those ABSs are at finite energies with no robust ZBPs observed at zero field. On the contrary, a ZBP robust in TG scan occurs at a field of 0.6 T as shown in Fig. 4(c). The B orientation is close to the x axis, different from the case of device A (which is near the y axis). This difference may be attributed to several correlated factors such as difference in spin-orbit interaction, g -factor anisotropy, and wire geometry etc. In Figure 4(d), we demonstrate its robustness in the SG scan.

Figure 4(e) shows the B evolution of this ZBP. At zero field, two subgap peaks near ± 0.2 mV split with increasing B and merge to zero around 0.5 T. This pattern is similar to that in device A. The difference is that this ZBP remains robust and non-split over an extended B range from 0.5 T to 1 T. Based on the dispersion of Andreev levels, the estimated g -factor is around 15. The ZBP’s field range of 0.5 T can be converted to a Zeeman energy of $\frac{1}{2}g\mu_B B \sim 0.225$ meV. This energy scale quantifies its robustness in B scan. Figure 4(f) shows another B scan at a different gate setting, where the ZBP reaches $2e^2/h$, see Fig. 4(g) for its line cut. This peak does not

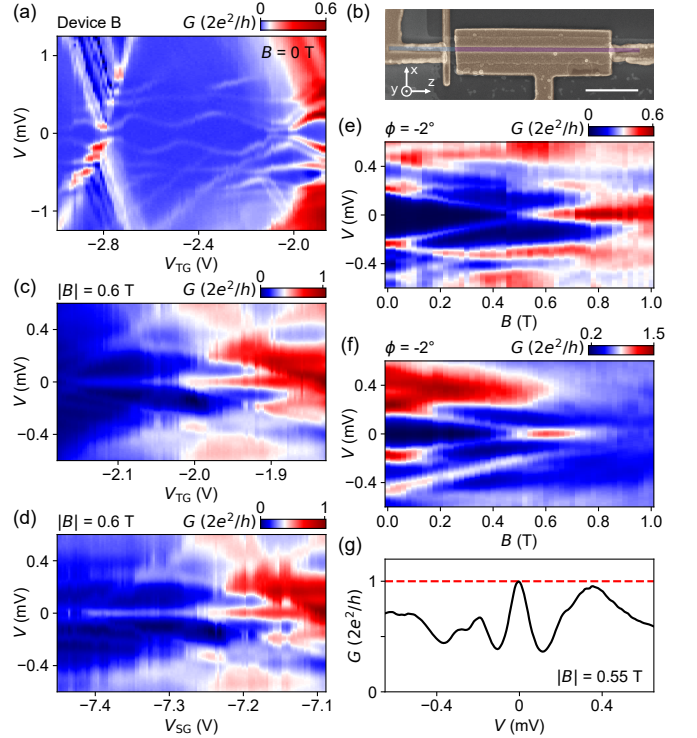


FIG. 4. Robust ZBP in a second device (device B). (a) G vs V and V_{TG} at 0 T. $V_{SG} = -7$ V. (b) False-colored SEM. Scale bar, 1 μm . (c) TG scan of the ZBP at 0.6 T. $V_{SG} = -7.2$ V. (d) SG scan of the ZBP at 0.6 T. $V_{TG} = -2$ V. (e-f) B scans of the ZBP. $V_{TG} = -2$ V, $V_{SG} = -7.45$ V for (e). $V_{TG} = -1.723$ V, $V_{SG} = -7$ V for (f). (g) A line cut from (f) at 0.56 T. $\phi = -2^\circ$, $\theta = 90^\circ$ for (c-f).

form a quantized plateau either. For additional B scans, see Fig. S5 in SM. Besides robust ZBPs, we also note the presence of non-robust ZBPs arising from sharp crossings of dot states [24], as demonstrated in Fig. S6 in SM.

In conclusion, we have demonstrated robust ZBPs in PbTe-Pb hybrid nanowires. Their robustness is evident in the presence of the ZBP (remaining non-split) over an extended range of the parameter space in gate voltages (both TG and SG scans) and magnetic field (both magnitude and angle rotation). While this robustness is a characteristic feature of Majorana zero modes, it is not conclusive evidence due to the inherent limitations of local tunneling spectroscopy. Our results establish a crucial necessary step towards realizing Majoranas in an emerging and scalable hybrid nanowire system. Future studies could focus on further optimizing nanowire quality — such as cleaner devices with fewer ABSs — and implementing three-terminal end-to-end correlation measurements, which could provide stronger evidence for Majorana modes.

Acknowledgment This work is supported by National Natural Science Foundation of China (92065206) and the Innovation Program for Quantum Science and Technology (2021ZD0302400). S.Y. acknowledges the China Postdoctoral Science Foundation

(Grant No. 2024M751610) and Postdoctoral Fellowship Program of China Postdoctoral Science Founda-

tion (Grant No. GZC20231368). Raw data and processing codes within this paper are available at <https://doi.org/10.5281/zenodo.14849781>

-
- [1] N. Read and D. Green, Paired states of fermions in two dimensions with breaking of parity and time-reversal symmetries and the fractional quantum hall effect, *Phys. Rev. B* **61**, 10267 (2000).
- [2] A. Y. Kitaev, Unpaired Majorana fermions in quantum wires, *Physics-Uspekhi* **44**, 131 (2001).
- [3] R. M. Lutchyn, J. D. Sau, and S. Das Sarma, Majorana fermions and a topological phase transition in semiconductor-superconductor heterostructures, *Phys. Rev. Lett.* **105**, 077001 (2010).
- [4] Y. Oreg, G. Refael, and F. von Oppen, Helical liquids and Majorana bound states in quantum wires, *Phys. Rev. Lett.* **105**, 177002 (2010).
- [5] C. Nayak, S. H. Simon, A. Stern, M. Freedman, and S. Das Sarma, Non-Abelian anyons and topological quantum computation, *Rev. Mod. Phys.* **80**, 1083 (2008).
- [6] V. Mourik, K. Zuo, S. M. Frolov, S. Plissard, E. P. Bakkers, and L. P. Kouwenhoven, Signatures of Majorana fermions in hybrid superconductor-semiconductor nanowire devices, *Science* **336**, 1003 (2012).
- [7] M. Deng, S. Vaitiekėnas, E. B. Hansen, J. Danon, M. Leijnse, K. Flensberg, J. Nygård, P. Krogstrup, and C. M. Marcus, Majorana bound state in a coupled quantum-dot hybrid-nanowire system, *Science* **354**, 1557 (2016).
- [8] Ö. Gül, H. Zhang, J. D. Bommer, M. W. de Moor, D. Car, S. R. Plissard, E. P. Bakkers, A. Geresdi, K. Watanabe, T. Taniguchi, *et al.*, Ballistic Majorana nanowire devices, *Nature Nanotechnology* **13**, 192 (2018).
- [9] H. Song, Z. Zhang, D. Pan, D. Liu, Z. Wang, Z. Cao, L. Liu, L. Wen, D. Liao, R. Zhuo, *et al.*, Large zero bias peaks and dips in a four-terminal thin InAs-Al nanowire device, *Phys. Rev. Research* **4**, 033235 (2022).
- [10] Z. Wang, H. Song, D. Pan, Z. Zhang, W. Miao, R. Li, Z. Cao, G. Zhang, L. Liu, L. Wen, *et al.*, Plateau regions for zero-bias peaks within 5% of the quantized conductance value $2e^2/h$, *Phys. Rev. Lett.* **129**, 167702 (2022).
- [11] T. Dvir, G. Wang, N. van Loo, C.-X. Liu, G. Mazur, A. Bordin, S. Haaf, J.-Y. Wang, D. Driel, F. Zatelli, *et al.*, Realization of a minimal Kitaev chain in coupled quantum dots, *Nature* **614**, 445 (2023).
- [12] M. Aghaee, A. Akkala, Z. Alam, R. Ali, A. Alcaraz Ramirez, M. Andrzejczuk, A. E. Antipov, P. Aseev, M. Astafev, B. Bauer, *et al.* (Microsoft Quantum), InAs-Al hybrid devices passing the topological gap protocol, *Phys. Rev. B* **107**, 245423 (2023).
- [13] H. Zhang, D. E. Liu, M. Wimmer, and L. P. Kouwenhoven, Next steps of quantum transport in Majorana nanowire devices, *Nature Communications* **10**, 5128 (2019).
- [14] E. Prada, P. San-Jose, M. W. de Moor, A. Geresdi, E. J. Lee, J. Klinovaja, D. Loss, J. Nygård, R. Aguado, and L. P. Kouwenhoven, From Andreev to Majorana bound states in hybrid superconductor-semiconductor nanowires, *Nature Reviews Physics* **2**, 575 (2020).
- [15] L. Kouwenhoven, Perspective on majorana bound-states in hybrid superconductor-semiconductor nanowires, *Modern Physics Letters B* **0**, 2540002 (0).
- [16] J. Liu, A. C. Potter, K. T. Law, and P. A. Lee, Zero-bias peaks in the tunneling conductance of spin-orbit-coupled superconducting wires with and without Majorana end-states, *Phys. Rev. Lett.* **109**, 267002 (2012).
- [17] E. Prada, P. San-Jose, and R. Aguado, Transport spectroscopy of NS nanowire junctions with Majorana fermions, *Physical Review B* **86**, 180503 (2012).
- [18] D. Rainis, L. Trifunovic, J. Klinovaja, and D. Loss, Towards a realistic transport modeling in a superconducting nanowire with Majorana fermions, *Physical Review B* **87**, 024515 (2013).
- [19] H. Pan and S. Das Sarma, Physical mechanisms for zero-bias conductance peaks in Majorana nanowires, *Phys. Rev. Research* **2**, 013377 (2020).
- [20] S. Ahn, H. Pan, B. Woods, T. D. Stanescu, and S. Das Sarma, Estimating disorder and its adverse effects in semiconductor majorana nanowires, *Phys. Rev. Materials* **5**, 124602 (2021).
- [21] S. Das Sarma and H. Pan, Disorder-induced zero-bias peaks in Majorana nanowires, *Phys. Rev. B* **103**, 195158 (2021).
- [22] C. Zeng, G. Sharma, S. Tewari, and T. Stanescu, Partially separated Majorana modes in a disordered medium, *Phys. Rev. B* **105**, 205122 (2022).
- [23] R. Hess, H. F. Legg, D. Loss, and J. Klinovaja, Trivial andreev band mimicking topological bulk gap reopening in the nonlocal conductance of long rashba nanowires, *Phys. Rev. Lett.* **130**, 207001 (2023).
- [24] E. J. Lee, X. Jiang, M. Houzet, R. Aguado, C. M. Lieber, and S. De Franceschi, Spin-resolved Andreev levels and parity crossings in hybrid superconductor-semiconductor nanostructures, *Nature Nanotechnology* **9**, 79 (2014).
- [25] J. Alicea, Y. Oreg, G. Refael, F. von Oppen, and M. P. A. Fisher, Non-Abelian statistics and topological quantum information processing in 1D wire networks, *Nature Physics* **7**, 412 (2010).
- [26] S. Plugge, A. Rasmussen, R. Egger, and K. Flensberg, Majorana box qubits, *New Journal of Physics* **19**, 012001 (2017).
- [27] T. Karzig, C. Knapp, R. M. Lutchyn, P. Bonderson, M. B. Hastings, C. Nayak, J. Alicea, K. Flensberg, S. Plugge, Y. Oreg, C. M. Marcus, and M. H. Freedman, Scalable designs for quasiparticle-poisoning-protected topological quantum computation with Majorana zero modes, *Phys. Rev. B* **95**, 235305 (2017).
- [28] S. Vaitiekėnas, A. M. Whiticar, M.-T. Deng, F. Krizek, J. E. Sestoft, C. J. Palmstrøm, S. Marti-Sanchez, J. Arbiol, P. Krogstrup, L. Casparis, and C. M. Marcus, Selective-area-grown semiconductor-superconductor hybrids: A basis for topological networks, *Phys. Rev. Lett.* **121**, 147701 (2018).
- [29] J. S. Lee, S. Choi, M. Pendharkar, D. J. Pennachio, B. Markman, M. Seas, S. Koelling, M. A. Verheijen, L. Casparis, K. D. Petersson, *et al.*, Selective-area chemical beam epitaxy of in-plane InAs one-dimensional chan-

- nels grown on InP(001), InP(111)b, and InP(011) surfaces, *Phys. Rev. Mater.* **3**, 084606 (2019).
- [30] R. L. M. O. het Veld, D. Xu, V. Schaller, M. A. Verheijen, S. M. E. Peters, J. Jung, C. Tong, Q. Wang, M. W. A. de Moor, B. Hesselmann, *et al.*, In-plane selective area InSb–Al nanowire quantum networks, *Communications Physics* **3**, 59 (2020).
- [31] C. Reeg, D. Loss, and J. Klinovaja, Finite-size effects in a nanowire strongly coupled to a thin superconducting shell, *Phys. Rev. B* **96**, 125426 (2017).
- [32] T. Kanne, M. Marnauza, D. Olsteins, D. Carrad, J. E. Sestoft, J. Bruijckere, L. Zeng, E. Johnson, E. Olsson, K. Grove-Rasmussen, and J. Nygård, Epitaxial Pb on InAs nanowires for quantum devices, *Nature Nanotechnology* **16**, 776 (2021).
- [33] M. Pendharkar, B. Zhang, H. Wu, A. Zarassi, P. Zhang, C. P. Dempsey, J. S. Lee, S. D. Harrington, G. Badawy, S. Gazibegovic, *et al.*, Parity-preserving and magnetic field-resilient superconductivity in InSb nanowires with Sn shells, *Science* **372**, 508 (2021).
- [34] M. S. Bjergfelt, D. J. Carrad, T. Kanne, E. Johnson, E. M. Fiordaliso, T. S. Jespersen, and J. Nygård, Superconductivity and parity preservation in As-grown In islands on InAs nanowires, *Nano Letters* **21**, 9875 (2021).
- [35] D. J. Carrad, M. Bjergfelt, T. Kanne, M. Aagesen, F. Krizek, E. M. Fiordaliso, E. Johnson, J. Nygård, and T. S. Jespersen, Shadow epitaxy for in situ growth of generic semiconductor/superconductor hybrids, *Advanced Materials* **32**, 1908411 (2020).
- [36] Z. Cao, D. E. Liu, W.-X. He, X. Liu, K. He, and H. Zhang, Numerical study of PbTe-Pb hybrid nanowires for engineering Majorana zero modes, *Phys. Rev. B* **105**, 085424 (2022).
- [37] Y. Jiang, S. Yang, L. Li, W. Song, W. Miao, B. Tong, Z. Geng, Y. Gao, R. Li, F. Chen, Q. Zhang, F. Meng, L. Gu, K. Zhu, Y. Zang, R. Shang, Z. Cao, X. Feng, Q.-K. Xue, D. E. Liu, H. Zhang, and K. He, Selective area epitaxy of PbTe-Pb hybrid nanowires on a lattice-matched substrate, *Phys. Rev. Materials* **6**, 034205 (2022).
- [38] J. Jung, S. G. Schellingerhout, M. F. Ritter, S. C. ten Kate, O. A. van der Molen, S. de Loijer, M. A. Verheijen, H. Riel, F. Nichele, and E. P. Bakkers, Selective area growth of PbTe nanowire networks on InP, *Advanced Functional Materials* **32**, 2208974 (2022).
- [39] Z. Geng, Z. Zhang, F. Chen, S. Yang, Y. Jiang, Y. Gao, B. Tong, W. Song, W. Miao, R. Li, *et al.*, Observation of Aharonov-Bohm effect in PbTe nanowire networks, *Phys. Rev. B* **105**, L241112 (2022).
- [40] S. C. ten Kate, M. F. Ritter, A. Fuhrer, J. Jung, S. G. Schellingerhout, E. P. A. M. Bakkers, H. Riel, and F. Nichele, Small charging energies and g-factor anisotropy in PbTe quantum dots, *Nano Letters* **22**, 7049 (2022).
- [41] Z. Zhang, W. Song, Y. Gao, Y. Wang, Z. Yu, S. Yang, Y. Jiang, W. Miao, R. Li, F. Chen, *et al.*, Proximity effect in PbTe-Pb hybrid nanowire Josephson junctions, *Phys. Rev. Mater.* **7**, 086201 (2023).
- [42] W. Song, Y. Wang, W. Miao, Z. Yu, Y. Gao, R. Li, S. Yang, F. Chen, Z. Geng, Z. Zhang, *et al.*, Conductance quantization in PbTe nanowires, *Phys. Rev. B* **108**, 045426 (2023).
- [43] Y. Gao, W. Song, S. Yang, Z. Yu, R. Li, W. Miao, Y. Wang, F. Chen, Z. Geng, L. Yang, *et al.*, Hard superconducting gap in PbTe nanowires, *Chinese Physics Letters* **41**, 038502 (2024).
- [44] Y. Wang, F. Chen, W. Song, Z. Geng, Z. Yu, L. Yang, Y. Gao, R. Li, S. Yang, W. Miao, *et al.*, Ballistic PbTe nanowire devices, *Nano Letters* **23**, 11137 (2023).
- [45] R. Li, W. Song, W. Miao, Z. Yu, Z. Wang, S. Yang, Y. Gao, Y. Wang, F. Chen, Z. Geng, *et al.*, Selective-area-grown PbTe-Pb planar Josephson junctions for quantum devices, *Nano Letters* **24**, 4658 (2024).
- [46] M. Gupta, V. Khade, C. Riggert, L. Shani, G. Menning, P. J. H. Lueb, J. Jung, R. Mélin, E. P. A. M. Bakkers, and V. S. Pribiag, Evidence for π -shifted cooper quartets and few-mode transport in pbte nanowire three-terminal josephson junctions, *Nano Letters* **24**, 13903 (2024).
- [47] W. Song, Z. Yu, Y. Wang, Y. Gao, Z. Li, S. Yang, S. Zhang, Z. Geng, R. Li, Z. Wang, F. Chen, L. Yang, W. Miao, J. Xu, X. Feng, T. Wang, Y. Zang, L. Li, R. Shang, Q. Xue, K. He, and H. Zhang, Reducing disorder in PbTe nanowires for Majorana research, *Nano Letters* **0**, null (2025).
- [48] Z. Geng *et al.*, Epitaxial Indium on PbTe nanowires for quantum devices, arXiv: 2402.04024 (2024).
- [49] Y. Wang, W. Song, Z. Cao, Z. Yu, S. Yang, Z. Li, Y. Gao, R. Li, F. Chen, Z. Geng, *et al.*, Gate-tunable subband degeneracy in semiconductor nanowires, *Proceedings of the National Academy of Sciences* **121**, e2406884121 (2024).
- [50] Y. Gao, W. Song, Z. Yu, S. Yang, Y. Wang, R. Li, F. Chen, Z. Geng, L. Yang, J. Xu, *et al.*, Squid oscillations in PbTe nanowire networks, *Phys. Rev. B* **110**, 045405 (2024).
- [51] Y. Gao *et al.*, Quantized Andreev conductance in semiconductor nanowires, arXiv: 2406.11211 (2024).
- [52] Z. Li *et al.*, Anisotropy of PbTe nanowires with and without a superconductor, arXiv: 2501.04345 (2025).
- [53] C. Moore, T. D. Stanescu, and S. Tewari, Two-terminal charge tunneling: Disentangling majorana zero modes from partially separated andreev bound states in semiconductor-superconductor heterostructures, *Physical Review B* **97**, 165302 (2018).
- [54] A. Vuik, B. Nijholt, A. Akhmerov, and M. Wimmer, Reproducing topological properties with quasi-Majorana states, *SciPost Physics* **7**, 061 (2019).
- [55] C. Moore, C. Zeng, T. D. Stanescu, and S. Tewari, Quantized zero-bias conductance plateau in semiconductor-superconductor heterostructures without topological Majorana zero modes, *Physical Review B* **98**, 155314 (2018).
- [56] C.-X. Liu, J. D. Sau, T. D. Stanescu, and S. D. Sarma, Andreev bound states versus Majorana bound states in quantum dot-nanowire-superconductor hybrid structures: Trivial versus topological zero-bias conductance peaks, *Physical Review B* **96**, 075161 (2017).

Supplemental Material for “Robust zero modes in PbTe-Pb hybrid nanowires”

Shan Zhang,^{1,*} Wenyu Song,^{1,*} Zonglin Li,^{1,*} Zehao Yu,^{1,*} Ruidong Li,¹ Yuhao Wang,¹ Zeyu Yan,¹ Jiaye Xu,¹ Zhaoyu Wang,¹ Yichun Gao,¹ Shuai Yang,¹ Lining Yang,¹ Xiao Feng,^{1,2,3,4} Tiantian Wang,^{2,4} Yunyi Zang,^{2,4} Lin Li,² Runan Shang,^{2,4} Qi-Kun Xue,^{1,2,3,4,5} Ke He,^{1,2,3,4,†} and Hao Zhang^{1,2,3,‡}

¹State Key Laboratory of Low Dimensional Quantum Physics,
Department of Physics, Tsinghua University, Beijing 100084, China
²Beijing Academy of Quantum Information Sciences, Beijing 100193, China
³Frontier Science Center for Quantum Information, Beijing 100084, China
⁴Hefei National Laboratory, Hefei 230088, China
⁵Southern University of Science and Technology, Shenzhen 518055, China

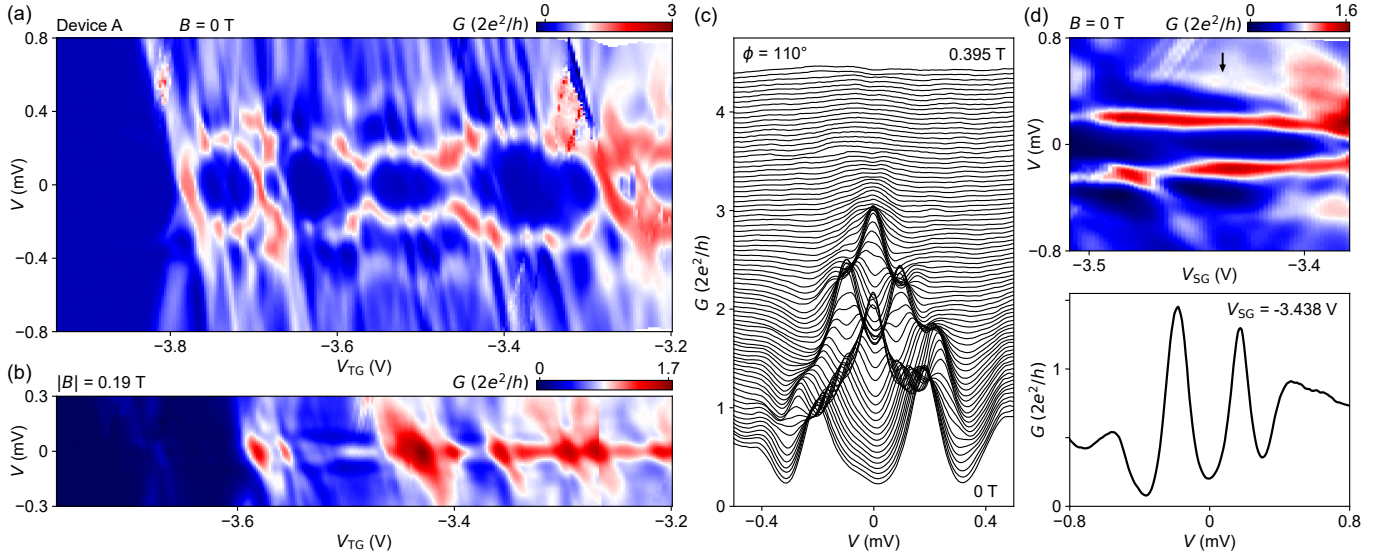


FIG. S1. (a) Tunneling spectroscopy of device A at zero field. The SG was scanned together with the TG, i.e. $V_{SG} = V_{TG}$. ABSs due to formation of unintentional quantum dots can be revealed. No robust ZBPs are observed at zero field. (b) Gate scan at 0.19 T over a larger range compared to Fig. 1(e). $\theta = 90^\circ$, $\phi = 110^\circ$. A robust ZBP can be revealed. (c) Waterfall plot of Fig. 1(b) with a vertical offset of $0.05 \times 2e^2/h$. (d) V_{SG} scan at zero field. $V_{TG} = -3.764$ V. The lower panel shows a vertical line cut (see the black arrow in the upper panel) of the two subgap peaks. The gap size is near 0.49 meV.

* equal contribution

† kehe@tsinghua.edu.cn

‡ hzquantum@mail.tsinghua.edu.cn

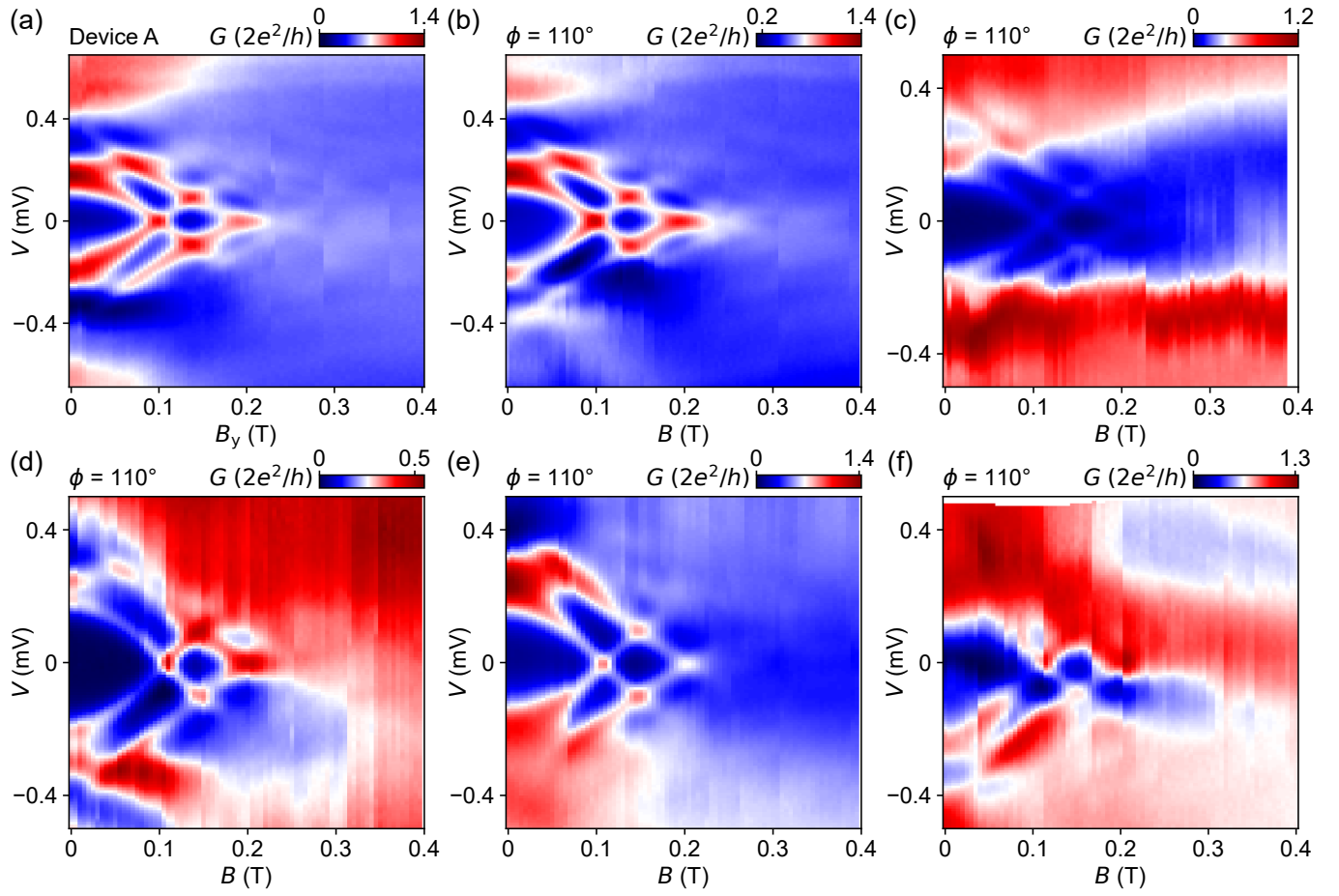


FIG. S2. Additional B scans at various gate voltages. $V_{TG} = -3.714$ V, -3.714 V, -3.9 V, -3.814 V, -3.814 V, -3.814 V, while $V_{SG} = -3.456$ V, -3.444 V, -4.151 V, -3.82 V, -3.93 V, -4.026 V, for panels (a-f). $\theta = 90^\circ$, $\phi = 110^\circ$ for (b-f), while for (a) B is aligned with the y axis. At some gate voltages, the B scan reveals no robust ZBPs.

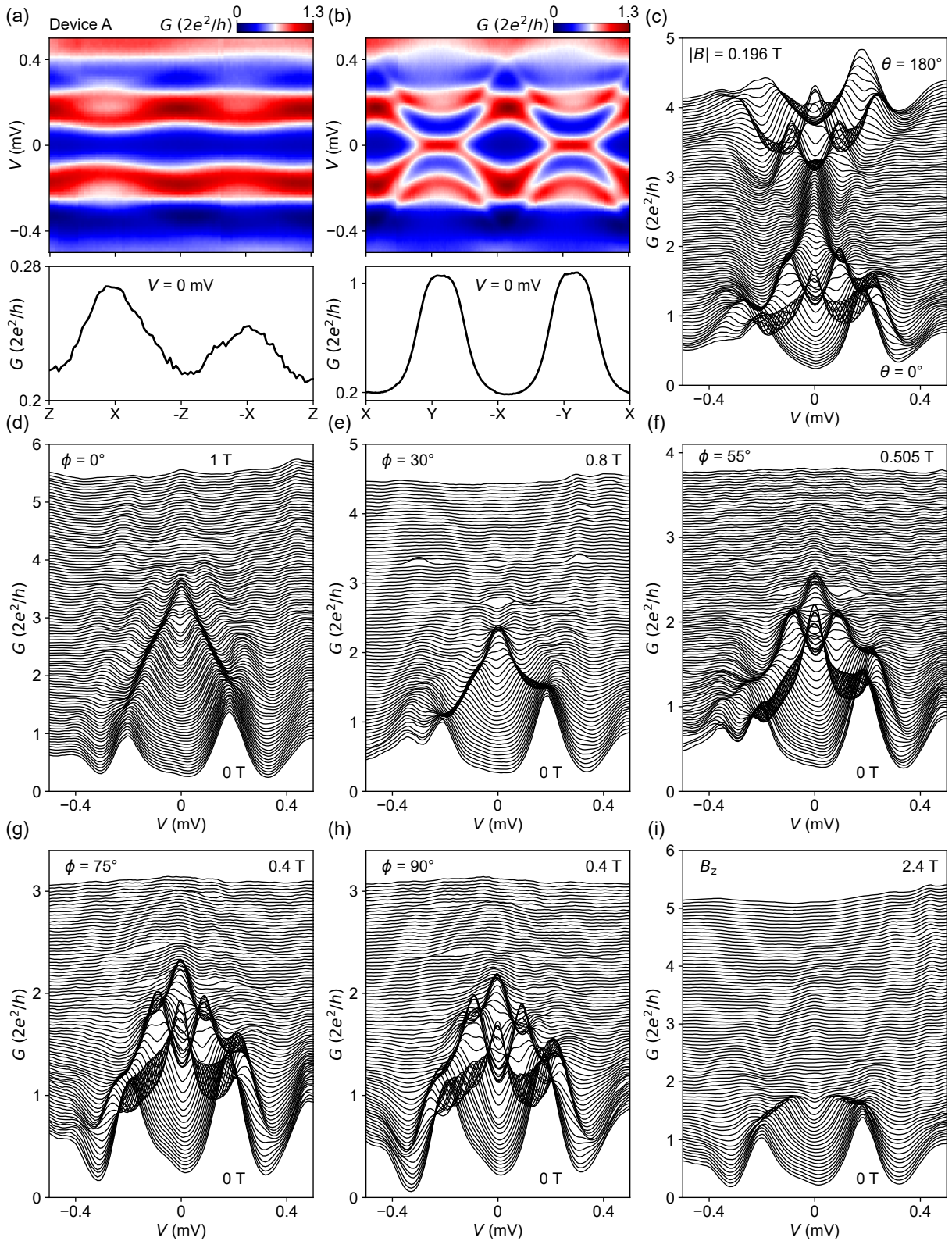


FIG. S3. (a) B rotation in the xz plane for $|B|$ fixed at 0.196 T. Gate settings are the same with that in Figs. 2(a-b). Lower panel, zero-bias line cut. (b) B rotation in the xy plane for $|B|$ fixed at 0.1 T. This ZBP corresponds to the non-robust one in Fig. 1(b). (c) Waterfall plot of Fig. 2(c) with a vertical offset of $0.04 \times 2e^2/h$. (d-i) Waterfall plots of Figs. 2(e-f). The vertical offsets (in units of $2e^2/h$) are 0.05, 0.05, 0.0325, 0.0325, 0.0325, and 0.06, respectively.

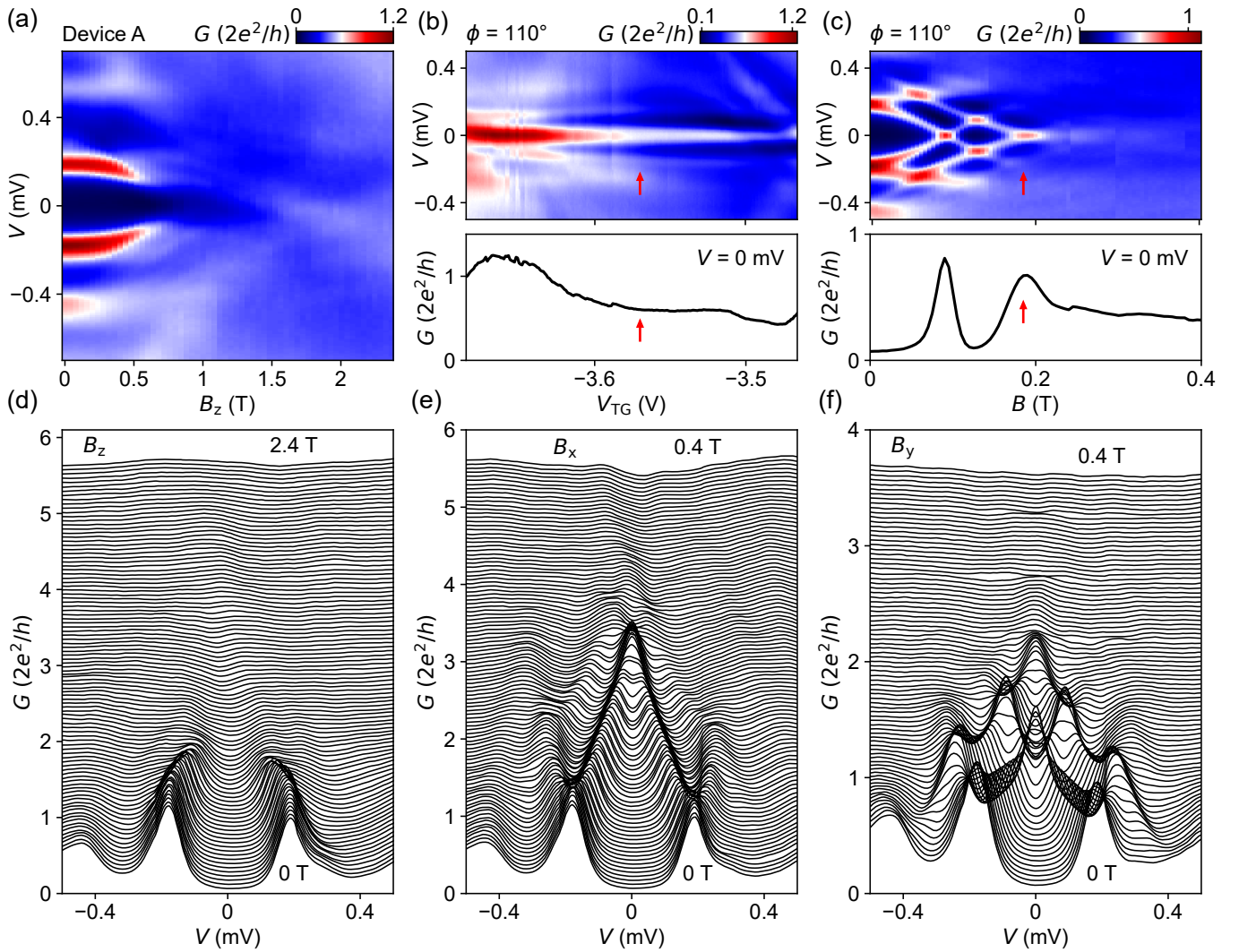


FIG. S4. (a) B_z scan of the ZBP in Figs. 3(a-b). No ZBP is revealed for B along this direction due to a small effective g -factor. (b) V_{TG} scan of the ZBP in Fig. 3. The lower panel shows the zero-bias line cut. The region labeled by the red arrow marks a “plateau-like” feature in V_{TG} scan. It is in fact not a true plateau, as the corresponding B scan shown in (c) does not reveal a plateau near this region (the red arrow). (c) Replot of Fig. 3(f) with zero-bias line cut shown in the lower panel. (d-f) Waterfall plots of panel (a), Fig. 3(a), and Fig. 3(b), respectively. The vertical offsets (in units of $2e^2/h$) are 0.055, 0.02, and 0.041, respectively.

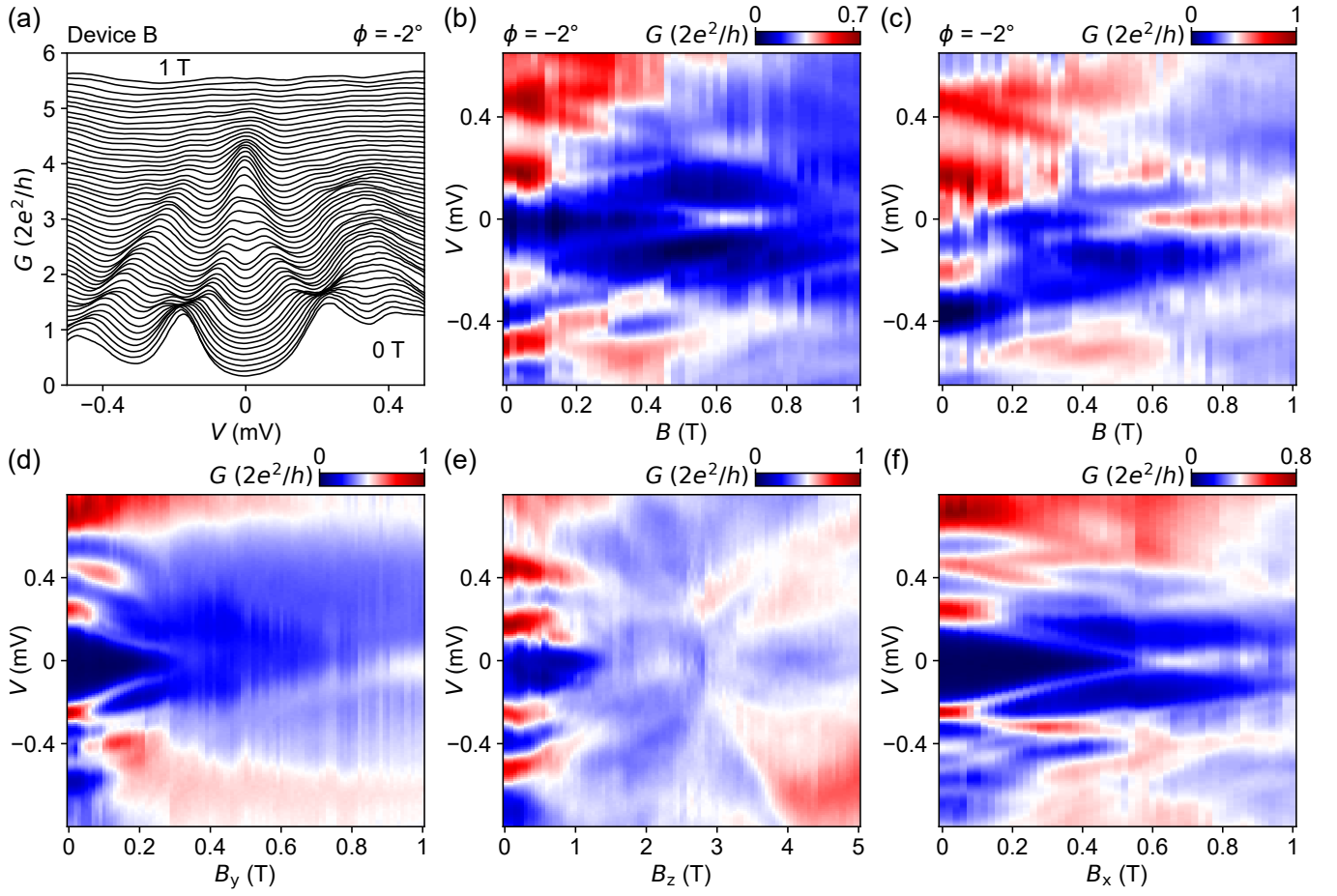


FIG. S5. (a) Waterfall plot of Fig. 4(f) with a vertical offset of $0.1 \times 2e^2/h$. (b-c) Two additional B scans in device B. $\theta = 90^\circ$, $\phi = -2^\circ$, $V_{TG} = -2$ V. $V_{SG} = -7.54$ V and -7.35 V, respectively. (d-f) B scans along three axes. $V_{SG} = -7$ V. $V_{TG} = -1.77$ V, -1.77 V, and -1.94 V, respectively.

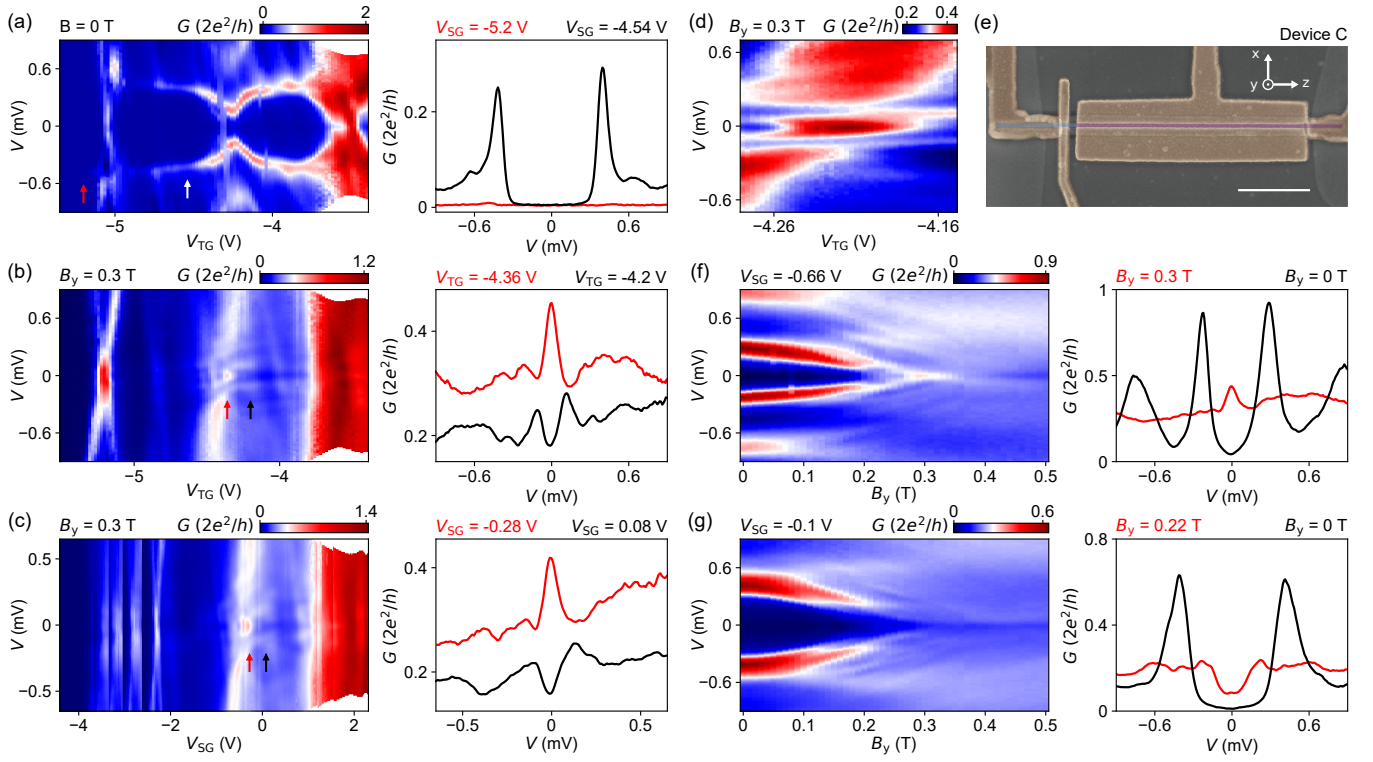


FIG. S6. An example of non-robust ZBP in device C. (a) Zero-field tunneling spectroscopy. $V_{SG} = 0$ V. Right panel, vertical line cuts at -5.2 V and -4.54 V (see the arrows in the left panel). (b-c) V_{TG} and V_{SG} scans at $B_y = 0.3$ T. $V_{SG} = 0$ V for (b) and $V_{TG} = -4.23$ V for (c). A ZBP is revealed (the red arrow), see the red line cuts in the right panels. This ZBP is non-robust and caused by a dot state crossing zero energy. The black curves correspond to the line cuts marked by the black arrows. (d) Fine measurement near this ZBP. $V_{SG} = -0.66$ V. The “tilted red region” indicates the dot state, which can be fine-tuned to zero by V_{TG} , causing a ZBP. (e) False-colored SEM of device C. Scale bar, 1 μm . (f) B_y scan of this ZBP. $V_{SG} = -0.66$ V. $V_{TG} = -4.216$ V. The ZBP is also non-robust in B scan and quickly splits with increasing B . Right panel, line cuts at 0 T and 0.3 T. (g) B_y scan at a different gate setting, revealing no ZBPs. $V_{SG} = -0.1$ V. $V_{TG} = -4.216$ V.